Separation Science and Technology
Publication details, including instructions for authors and subscription information:
http://www.informaworld.com/smpp/title~content=t713708471

Prediction Model for Transmembrane Pressure in a Submerged Hollow-Fiber Microfiltration Membrane

Hwan-Mook Lee[a]; Chung-Hak Lee[a]; Kun Yong Chung[b]; Sangho Lee[c]
[a] School of Chemical Engineering, Seoul National University, Seoul, South Korea [b] Department of Chemical Engineering, College of Engineering, Seoul National University of Technology, Seoul, South Korea [c] Construction Environment Department, Korea Institute of Construction Technology, Kyeonggi-Do, South Korea

Online publication date: 08 July 2010

To cite this Article Lee, Hwan-Mook , Lee, Chung-Hak , Chung, Kun Yong and Lee, Sangho(2005) 'Prediction Model for Transmembrane Pressure in a Submerged Hollow-Fiber Microfiltration Membrane', Separation Science and Technology, 39: 8, 1833 — 1856
To link to this Article: DOI: 10.1081/SS-120037392
URL: http://dx.doi.org/10.1081/SS-120037392

SEPARATION SCIENCE AND TECHNOLOGY
Vol. 39, No. 8, pp. 1833–1856, 2004

Prediction Model for Transmembrane Pressure in a Submerged Hollow-Fiber Microfiltration Membrane

Hwan-Mook Lee,[1] Chung-Hak Lee,[1,*] Kun Yong Chung,[2] and Sangho Lee[3]

[1]School of Chemical Engineering, Seoul National University, Seoul, South Korea
[2]Department of Chemical Engineering, College of Engineering, Seoul National University of Technology, Seoul, South Korea
[3]Construction Environment Department, Korea Institute of Construction Technology, Kyeonggi-Do, South Korea

ABSTRACT

In this study, a model equation was derived for a submerged, hollow-fiber microfiltration (MF) membrane under constant flux. The validity of model equation was examined in two aspects: different feed water concentration and membrane pore size. When the concentration of starch solution (feed water) was varied from 1.5 to 9.0 g/L, the model equation predicted transmembrane pressure (TMP) variation at the precision of 99% within that

*Correspondence: Chung-Hak Lee, School of Chemical Engineering, Seoul National University, Seoul 151-744, South Korea; Fax: +82-2-888-1604; E-mail: leech@snu.ac.kr.

DOI: 10.1081/SS-120037392 0149-6395 (Print); 1520-5754 (Online)

range of concentration. In the cases of a different nominal membrane pore size (0.1 and 0.4 μm), it was capable of predicting TMP variation in a good manner. From experimental TMP data, it was ascertained that different pore sizes of membrane hardly affected filtration time. At the same time, TMP, flux, and total resistance distributions along the membrane length, which cannot be measured directly, could be calculated using the model equation.

Key Words: Submerged type; Constant flux; Model equation; Hollow fiber; Transmembrane pressure.

INTRODUCTION

As we come to the 21st century, a brilliant industrial era, factors causing contamination of potable water quality become manifold and a conventional water treatment system cannot satisfy all the new stringent regulations needed to produce drinking water of good quality. Therefore, a water treatment system using a membrane process has come forth as one way of advanced drinking water treatment in place of conventional water treatment system using the typical coagulation–sedimentation–disinfection processes. Membrane processes appear to be well suited to meet these more stringent requirements since they are capable of removing suspended solids and microorganisms and pathogens, such as *Giardia* and *Cryptospordium*, in a reliable and cost-effective fashion,[1,2] which cannot be fulfilled by the old-fashioned processes. Among them, submerged microfiltration has several potential advantages compared to cross-flow membrane processes, which were used widely in times past, such as compactness of system, easiness of operation, and small capital cost. Furthermore, it reduces the energy consumption by the recirculation pump used in a cross-flow microfiltration process.[3]

Although it has many advantages over a conventional water treatment system, the membrane process has a critical problem to be solved, that is, the fouling of the membrane surface causing increase of transmembrane pressure (TMP), even though many studies have been attempted. So, it is a very important affair to predict TMP variation, if the TMP profile of some operations can be expected approximately, it would be greatly helpful to economical and effective process operation. There are several studies of membrane fouling phenomena in the case of a dead-end type,[4] constant-pressure driven filtration of water.[5] However, there are few studies of modeling of membrane fouling mechanisms in the case of the submerged type, hollow-fiber filtration under constant flux operation. Moreover, they

MARCEL DEKKER, INC.
270 Madison Avenue, New York, New York 10016

are at the level of developing model equations and just fitting experimental data so that they cannot predict experimental results under other conditions.

Because of this, the aim of this study was to elucidate the principle of the membrane fouling mechanism and develop a useful model equation to predict TMP variation caused by fouling under constant flux operation based on the work of Hermia[5] and Fujita.[6] As a representation of organic matter existing in water, potato starch solution was used as a feed water. TMP profiles for different concentrations of feed solution and different nominal membrane pore sizes were evaluated to check the possibilities of applying a model equation to analyze and predict the real fouling phenomenon.

THEORETICAL ANALYSIS

Governing Equations

Typical hollow fiber in a submerged membrane module is characterized by internal and external diameters (D_i and D_o), fiber and potted lengths (L and L_p), as shown in Fig. 1. Both ends of a fiber are potted while the insides are open. Hence, the permeate (J, v), by suction from the surface to the inside of a hollow fiber, can flow through the inside of a fiber. As the hydrodynamic behavior is symmetrical on the longitudinal center of a fiber, only the half of a fiber with one side sealed was used, which is shown in Fig. 1.

The governing equations for pressure (p), flow velocity (v), and permeate flux (J) based on the mass, energy balance, and Darcy's law,[6] were proposed as follows.

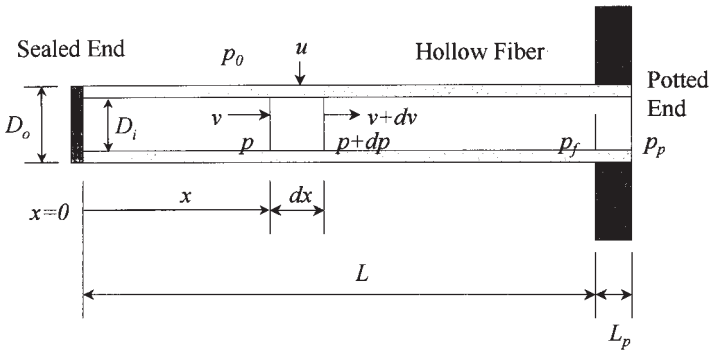

Figure 1. Permeation flow through the hollow-fiber membrane.

For a differential element (dx), the energy balance coupled with the Hagen–Poiseuille equation becomes

$$p + \frac{\rho v^2}{2} = (p + dp) + \frac{\rho(v + dv)^2}{2} + \frac{32\mu v}{D_i^2} dx \tag{1}$$

where p is the pressure, D_i is the inner diameter of hollow fiber membrane, g is the gravitational acceleration, ρ is the density of the fluid that passes through the lumen, μ is the viscosity of the fluid, and x is the distance from the sealed end (SE) of the fiber. This equation is the basic governing equation for the model.

Assuming that the square of differential term $[\rho(dv)^2/2]$ is negligible, dividing Eq. (1) by dx, the pressure gradient along the x direction, dp/dx, is expressed as:

$$\frac{dp}{dx} = -\rho v \frac{dv}{dx} - \frac{32\mu v}{D_i^2} \tag{2}$$

from the mass balance in the differential volume, the relationship between v and u is

$$\frac{\pi}{4} D_i^2 (v + dv) - \frac{\pi}{4} D_i^2 v = \pi D_o J dx \tag{3}$$

where J is the permeate flux and D_o is the outer diameter of the fiber. Simplifying Eq. (3) and dividing it by dx, the velocity gradient along the x direction is obtained.

$$\frac{dv}{dx} = \frac{4 D_o J}{D_i^2} = a_1 J \tag{4}$$

Using Eqs. (2) and (4), the pressure gradient along the x direction is

$$\frac{dp}{dx} = \frac{32\mu v}{D_i^2} \left(-\frac{\rho D_o J}{8\mu} - 1 \right) \tag{5}$$

$\rho D_o J/8\mu$ has the maximum value of 2.602×10^{-3} and this value can be neglected. Thus, the pressure gradient in a hollow fiber is expressed as:

$$\frac{dp}{dx} = \frac{32\mu v}{D_i^2} = -a_2 v \tag{6}$$

The permeate flux J is expressed by Darcy's law

$$J = k(p_o - p) \tag{7}$$

Marcel Dekker, Inc.
270 Madison Avenue, New York, New York 10016

where k is the hydrodynamic permeability and p_o is the atmospheric pressure. For a constant flux operation, the average flux J_{avg} is expressed as:

$$J_{avg} = \frac{v_f D^2}{4 D_o L} = \frac{v_f}{a_1 L} \tag{8}$$

and the velocity of fluid at the end of the membrane v_f should be constant. Besides, when the fluid reaches the potted area of membrane, there is no velocity variation but only pressure loss occurs, which can be calculated using the Hagen–Poieuille equation.

$$p_p = p_f - \frac{32 \mu v_f (L_p + L_t)}{D_i^2} = p_f - a_2 v_f (L_p + L_t) \tag{9}$$

where p_p is the pressure at the exit of membrane module, p_f is the pressure at the beginning of potted area, L_p is the length of potted area, and L_t is the length of tubing between the end of potted area and where the pressure gauge is located.

Filtration Model

There are several kinds of filtration models to explain the fouling mechanism, such as complete blocking, standard blocking, intermediate blocking, and cake filtration models.[4,5] Among them, a standard blocking model can fit our experimental results well. We developed a model equation of a constant flux operation based on the standard blocking model. In deriving the standard blocking model, it is assumed that pore volume decreases proportionally to filtrate volume by particle deposition on the pore walls. The membrane is assumed to consist of a set of pores of constant diameter. The length of the pores also being assumed constant, the decrease of pore volume will be equal to the decrease of pore section. A brief sketch of a cylindrical pore is shown in Fig. 2.

A mass balance on solid particles yields,

$$N^*(-2\pi r dr) l = C dV_F \tag{10}$$

where r is the radius of decreased pore, N^* is the total number of pores, l is the pore length, C is the volume of particles deposited by unit volume of filtrate, and dV_F represents the unit filtrate volume.

MARCEL DEKKER, INC.
270 Madison Avenue, New York, New York 10016

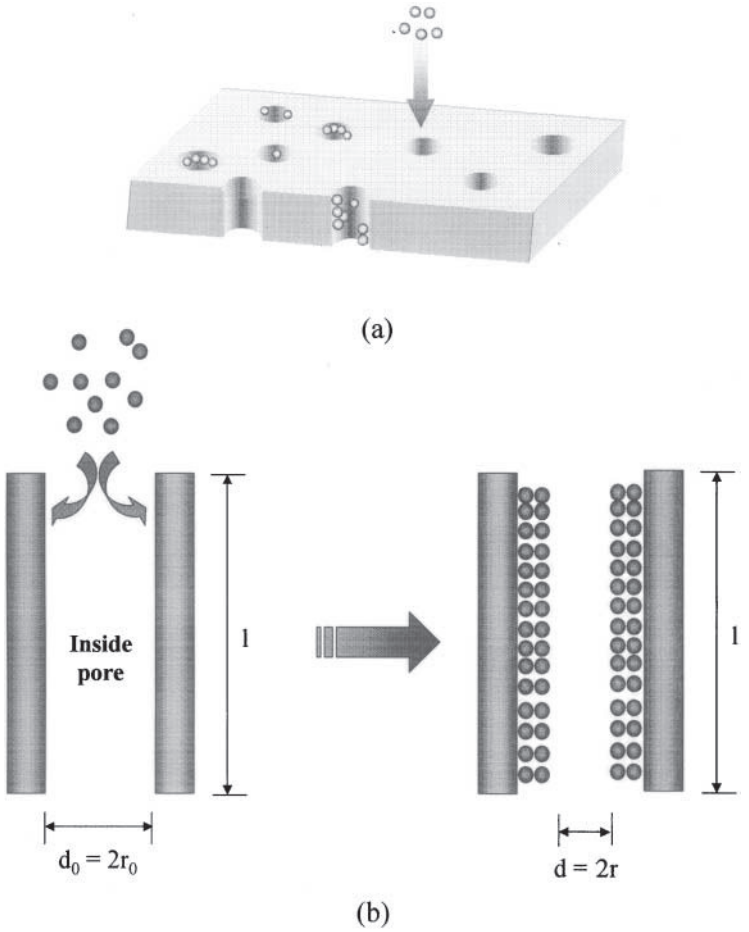

Figure 2. A schematic diagram of a cylindrical pore. (a) Uniform membrane pores and foulants inside the pores. (b) Magnified picture of one pore.

Integrating this relation, we obtain

$$N^* \pi (r_0^2 - r^2) l = C V_F \tag{11}$$

making use of Hagen–Poiseuille's equation to find the initial flow rate

$$Q_0 = N^* \left(\frac{\pi}{8} \frac{r_0^4 p}{\mu l} \right) \tag{12}$$

Marcel Dekker, Inc.
270 Madison Avenue, New York, New York 10016

although time passes, other conditions, except pore radius, are constant,

$$\frac{Q}{Q_0} = \left(\frac{r}{r_0}\right)^4 = \left(1 - \frac{K_{sb} V_F}{2}\right)^2 = \frac{J}{J_0} \tag{13}$$

where

$$K_{sb} = \frac{2C}{\pi l N^* r_0^2} \tag{14}$$

from Eqs. (7) and (13), we can obtain

$$J = J_0 \left(1 - \frac{K_{sb} V_F}{2}\right)^2 = k_0 (p_o - p) \left(1 - \frac{K_{sb} V_F}{2}\right)^2 \tag{15}$$

where Q is the flow rate, Q_0 is the initial flow rate, J is the permeate flux, J_0 is the initial permeate flux, r_0 is the initial pore radius, and K_{sb} is the standard blocking model constant. Equation (15) is the general form of a standard blocking model equation. Equation (15) is coupled with Eq. (7) to yield the hydrodynamic permeability k as a function of V_F or time.

$$k = k_0 \left(1 - \frac{K_{sb} V_F}{2}\right)^2 \tag{16}$$

As V_F is the function of time, Eq. (16) shows the time-dependence of k, which contains the fouling effect of standard blocking as time passes.

Calculation Method

As there are three unknowns (p, v, J) to solve simultaneously, three equations [Eqs. (4), (6), and (7)] are needed. For Eqs. (4) and (6), two boundary conditions about v and p are needed. At the beginning of membrane module ($x = 0$), the fluid velocity is zero. When the operation is a constant flux operation, the velocity of the fluid at the end of the membrane (v_f) is constant, which is obtained from Eq. (8), i.e., when x is L, $v = v_f$. As one more condition about p is needed, the initial TMP ($x = 0$) is supposed with an appropriate value. Then, putting the assumed initial TMP into Eq. (7), we can obtain the flux (J) of the differential volume. This flux is used in Eq. (4) to yield the velocity increment, which is used to get the pressure gradient, which is, the start of the calculation at the next differential volume. When the terminal exit velocity (v_f, $x = L$) is obtained in this calculation, that value and v_f obtained from Eq. (8) are compared to check the suitability of the presumed initial TMP value. When the two values are

Marcel Dekker, Inc.
270 Madison Avenue, New York, New York 10016

different, a new initial TMP is assumed again, based on the relationship of p and v, iteration is repeated when the two velocities come into the error tolerance range. Then, we can conclude that the initial TMP is assumed precisely. This value automatically becomes the other condition about pressure. With this assumed initial TMP value and the initial velocity, flux (J) and the gradient of velocity (v) and pressure (p) of differential membrane module (dx) are calculated to the end of membrane module at certain fixed time. k of each differential volume is calculated from the standard blocking model equation using the obtained flux of that differential volume. The acquired k values become the initial k values of each differential volume at the next differential time. In this course, the best-fitting K_{sb} value of a given experimental TMP data curve is the one that makes the value of $1 - r^2$ near zero. This process can be aided by MATLAB software.

EXPERIMENTAL

Materials

A potato starch was chosen as a solute of feed solution because its particle size is proper to cause standard blocking for fiber microfilteration (MF) membranes. It was used a representative model for organic matter in raw water or wastewater. For the experiment about variation of the concentration of feed water, a different mass of potato starch was mixed with ultra pure water, 1 L of 18 MΩ cm, made in a distillatory apparatus (Barnstead, USA) to yield different concentrations of starch solution (1.5–9.0 g/L). Under the same condition of feed water, 0.1- and 0.4-μm nominal pore size hollow fiber membranes (manufactured by Mitsubishi Rayon, Japan) were used to investigate the dependence of K_{sb} on the different pore size.

The specifications of the two membranes are listed in Table 1. As the outer diameters of two membrane are not equal, each module has different

Table 1. Specifications of hydrophilic polyethylene hollow fiber membranes.

Membranes	0.1-μm membrane	0.4-μm membrane
Surface area (A_t)	60 cm^2	60 cm^2
Outer diameter (D_o)	410 μm	540 μm
Inner diameter (D_i)	270 μm	360 μm
Fiber length (L)	10.0 cm	10.0 cm
Potted area length (L_p)	2.0 cm	2.0 cm

Marcel Dekker, Inc.
270 Madison Avenue, New York, New York 10016

number of fiber stands so as to have same total area (60 cm^2). Forty eight strands of fiber are assembled in 0.1-μm membrane; and 36 strands are in a 0.4-μm membrane. The length of the membrane module was 10 cm, and total area of the module was 0.006 cm^2. The one side of membrane module was sealed with epoxy (SE), and suction was performed through the other side [potted end (PE)].

Operation of Submerged Microfiltration System

A brief schematic of the experimental setup is shown in Fig. 3. The feed solution was mixed by a magnetic stirrer at 750 rpm for 10 min before suction started. The operation was in a total-recycle mode, operation flux was fixed at 100 LMH in all concentrations, and a transducer connected to an IBM PC measured the increase of TMP. When the TMP was 30 kPa, the limit of the recommended operating pressure, suction was stopped. One K_{sb} determines one theoretical fitting curve. Therefore, with these TMP data, we can

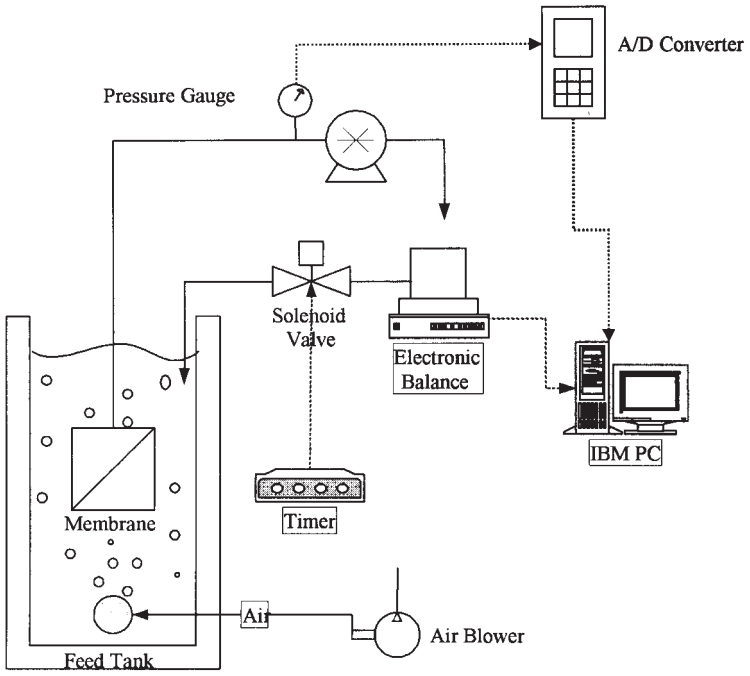

Figure 3. A schematic diagram of an experimental device.

choose K_{sb} which fits each experimental TMP datum curve best by least squares method using MATLAB software.

Resistance Analysis

A resistance R is expressed as:

$$R = \frac{P}{(\mu \cdot J)} \tag{17}$$

where P is a TMP, μ is a viscosity of permeate, and J is a flux. Putting TMP data of distilled water at a fixed flux (100 LMH) into Eq. (17), we can acquire an R_m value. With the membrane of completed experiment, R_t is obtained, then removing cake layer gives $R_t - R_c$ resistance. Finally, R_f can be obtained by $R_t - R_c - R_m$.[7,8]

When the particle size of the potato starch solution was measured by Mastersizer (Malvern, UK), it showed a typical bipeak size distribution. It is very feasible that standard blocking should occur according to the particle size distribution of submicrometer range. But also, there is another peak of size range (10–30 μm) that may form a cake layer on the membrane surface. So the significance of cake filtration effects was checked in this experiment by calculating R_c (cake resistance) and R_f (fouling resistance) and comparing their sizes, as shown in Table 2.

For the cases of 0.1- and 0.4-μm membranes and 3.0 g/L starch filtration system at 100 LMH, R_f is about 45% of total resistance, but R_c is about 2% of total resistance. R_c is merely 4–5% of R_f, so a standard blocking mechanism was dominant in this experimental system, and the cake filtration mechanism was negligible.

Table 2. Various resistances.

	0.1-μm membrane	0.4-μm membrane
R_m (m^{-1})	2.71×10^{11}	2.01×10^{11}
R_t ($=R_m + R_f + R_c$) (m^{-1})	5.08×10^{11}	3.96×10^{11}
$R_t - R_c$ ($= R_m + R_f$) (m^{-1})	4.96×10^{11}	3.87×10^{11}
R_c (1/m)	1.13×10^{10}	8.43×10^{9}
R_f (1/m)	2.25×10^{11}	1.86×10^{11}
R_m/R_t (%)	53.4	50.8
R_c/R_t (%)	2.2	2.1
R_f/R_t (%)	44.4	47.0
R_c/R_f (%)	5.00	4.53

MARCEL DEKKER, INC.
270 Madison Avenue, New York, New York 10016

Measurement of Pore Size Distribution

In general, pore size of a membrane has a wide distribution. Also the shape of pores is very irregular. So it is quite difficult to measure an accurate pore size. Many techniques are available for the measurement of porosity: mercury penetration, gas adsorption or permeation, and combined methods of "bubble" and solvent permeability.[9] Among them, the last method, called the "bubble pressure" method (or liquid–liquid porosimetry), can evaluate the pore size by measurement of the pressure necessary to force a gas or a liquid through the water-swollen membranes.[9,10]

For 0.1- and 0.4-μm MF membranes, the pore sizes can be measured under low operating pressure by the liquid–liquid porosimetry method using two immiscible liquids A and B. It was assumed that hydrophilic MF had cylindrical pores and pore size distribution as shown in Fig. 4. The upper section of the measurement cell was filled with an alcoholic mixture (A), and the lower was connected with a reservoir, filled with distilled water (B), and a pressure with which liquid B can push liquid A in the very pore is expressed as:

$$r = \frac{2\delta}{P} \tag{18}$$

where r is a pore radius, δ is an interfacial tension, and subscripts (1, 2, 3,. . .) mean various sizes of pores. When the pressure is increased from ΔP_1 to ΔP_2,

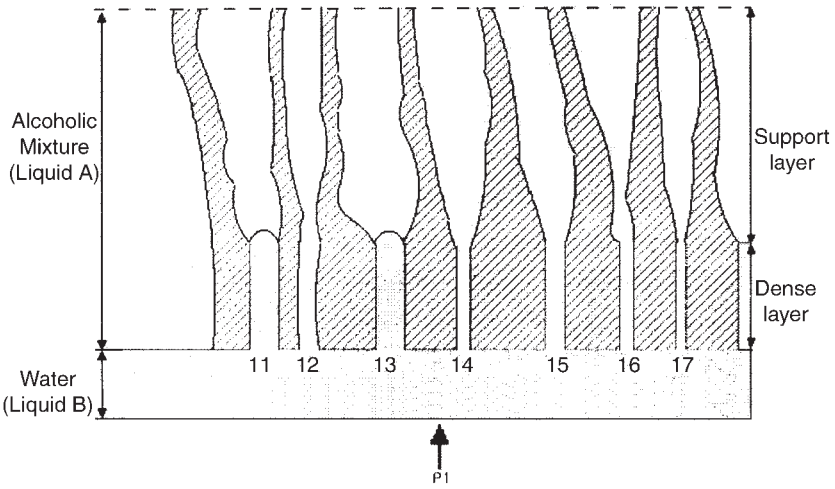

Figure 4. A draft of pore size distribution measurement.

the number of pores that liquid B displaced liquid A and with sizes between r_1 and r_2 can be expressed as:

$$n_{12} = \frac{\mu L \Delta P_{12}^3}{2\pi\delta^4} Q_{12} \tag{19}$$

where μ is a fluid viscosity and L is a thickness of the dense layer of membrane, $\Delta P_{12} = (\Delta P1 + \Delta P_2)/2$, n_{12} and Q_{12} represent the difference of pores and flow rate when the pressure is increased from ΔP_1 to ΔP_2. By putting pressure and flow rate data into Eqs. (18) and (19), size distribution of membrane pores can be measured. At this moment, the data had an S-shaped curve (refer to Fig. 5). It initially increased curvedly when liquid A in the pores was replaced with liquid B but increased straightly, by Hagen–Poiseuille equation after liquid B filled all pores of membrane.

To get N^* value, the liquid–liquid porosimetry method[9,10] was adopted. The experimental data reported are related to the following pairs of liquids recommended by some investigators in a study of biological membranes:[11] distilled water—mixture of isobutanol, methanol, and water (5 : 1 : 4 v/v) ($\delta = 0.8$ dyne/cm).

TMP and flux data used for the method are shown in Fig. 5. Throughout the liquid–liquid porosimetry method, the number of pores and pore size distribution data can be known. The data are listed in Tables 3 and 4. Through the calculation for N^*, it was found that r_0 values are somewhat different from the values reported by the maker. This is resulted from the fact that the r_0 values calculated by a liquid–liquid porosimetry method are based on the assumption that pores have a cylindrical form. So, as r_0 values are used for calculation of standard blocking model that assumes membrane pore is a cylindrical form, it is

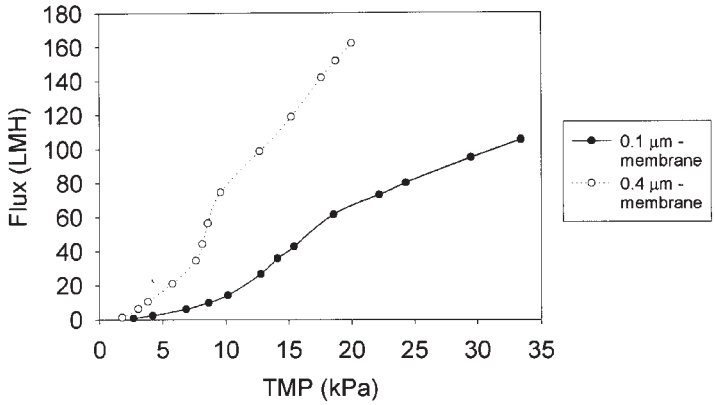

Figure 5. TMP vs. flux data used in the liquid–liquid porosimetry method.

MARCEL DEKKER, INC.
270 Madison Avenue, New York, New York 10016

Table 3. The number of pores and pore size distribution calculated by liquid–liquid porosimetry method of 0.1-μm membrane.

Pore diameter (μm)	Number ($\times 10^{15}$, per cm^2)	Fraction (%)
0.17–0.21	4.638	57.3
0.21–0.23	1.094	13.5
0.23–0.25	1.125	13.9
0.25–0.32	0.932	11.5
0.32–0.37	0.184	2.3
0.37–0.47	0.088	1.1
0.47–0.77	0.032	0.4
0.77–1.20	0.003	0.04
Mean diameter: 0.22 μm	Total number: 8.095×10^{15}	Total percentage: 100%

reasonable that r_0 values calculated by liquid–liquid porosimetry method should be chosen as r_0 of membranes with pores that are postulated to be a cylinder.

RESULTS AND DISCUSSION

Composition of Standard Blocking Constant

The standard blocking constant (K_{sb}) is expressed as Eq. (14).[5] That equation means that K_{sb} is proportional to C and is in inverse proportion to r_0^2. If the model equation reflects reality well, then it can be predicted that when the concentration of feed water or the initial membrane pore radius is changed, K_{sb} will be changed as defined in Eq. (14). Thus, there are two

Table 4. The number of pores and pore size distribution calculated by liquid–liquid porosimetry method of 0.4-μm membrane.

Pore radius (μm)	Number ($\times 10^{14}$, per cm^2)	Fraction (%)
0.34–0.37	8.810	44.3
0.37–0.40	4.517	22.7
0.40–0.42	3.046	15.3
0.42–0.56	2.605	13.1
0.56–0.84	0.738	3.7
0.84–1.05	0.107	0.5
1.05–1.81	0.045	0.2
Mean diameter: 0.41 μm	Total number: 1.987×10^{15}	Total percentage: 100%

MARCEL DEKKER, INC.
270 Madison Avenue, New York, New York 10016

kinds of experiment, one is about the change of concentration of feed water, the other involves the difference of the initial pore radius. The K_{sb} value that defines one curve was obtained by the least squares method with MATLAB software. Figure 6 shows the experimental TMP increase curve with time course (circle dots for 0.1 μm, stars for 0.4 μm) and with fitting curves (line) that were obtained by the least squares method in each pore size case. TMP profiles

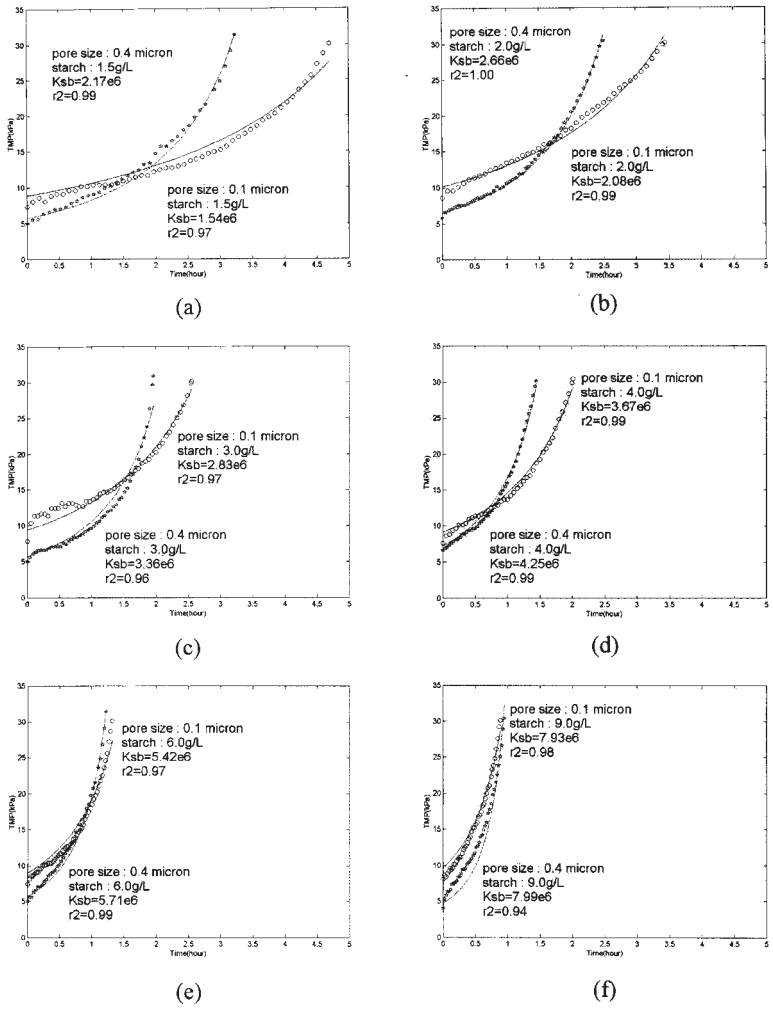

Figure 6. Experimental TMP data and fitting curves. Starch concentration of (a) 1.5 g/L (b) 2.0 g/L, (c) 3.0 g/L, (d) 4.0 g/L, (e) 6.0 g/L, and (f) 9.0 g/L.

MARCEL DEKKER, INC.
270 Madison Avenue, New York, New York 10016

were obtained when the maximum TMP reached 30 kPa at constant flux (100 LMH). Starch concentration varied from 1.5 to 9.0 g/L and 0.1- and 0.4-μm membranes were used at each concentration of starch solution.

Flux and TMP Distribution

The permeate flux and pressure distribution within a hollow fiber were calculated numerically using the standard blocking constant obtained from the regression analysis of experimental data. Flux distribution, TMP distribution, and total resistance (R_t) at fixed time along the hollow fiber membrane are shown in Figs. 7–9, respectively. Each curve was obtained at fixed time intervals, which started from 1/6 time of total suction time, which is needed for TMP to reach 30 kPa, to whole suction time (6/6 time), i.e., operating time (t) is expressed as dimensionless time, $\theta = t/T$, where T is the total suction time. Suction was executed at the PE ($x = L$ position) and the opposite side (SE, $x = 0$ position) was sealed with epoxy. According to the results, shown in Fig. 8, TMP increases from SE to PE at each fixed time. Because suction was performed at PE, more strong pressure is applied to that side of membrane.

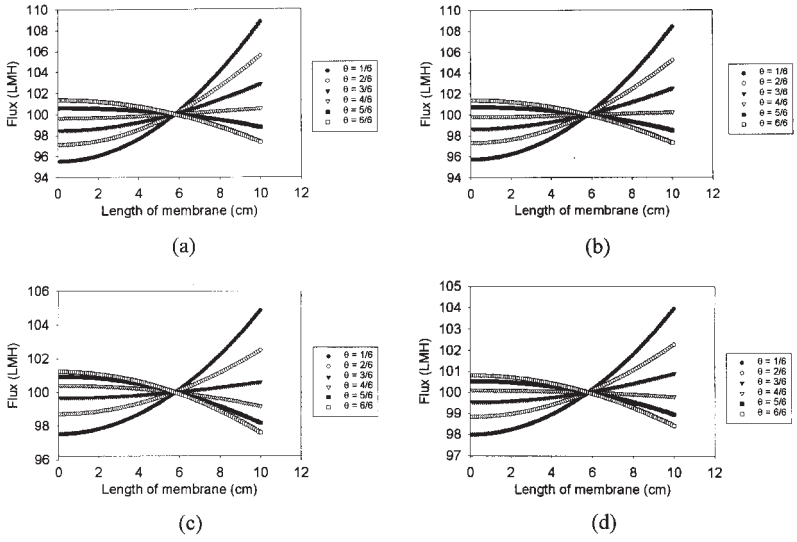

Figure 7. Flux distribution along the membrane length: (a) a 0.1-μm membrane, 1.5 g/L starch concentration; (b) a 0.1-μm membrane, 4.0 g/L starch concentration; (c) a 0.4-μm membrane, 1.5 g/L starch concentration; and (d) a 0.4-μm membrane, 4.0 g/L starch concentration.

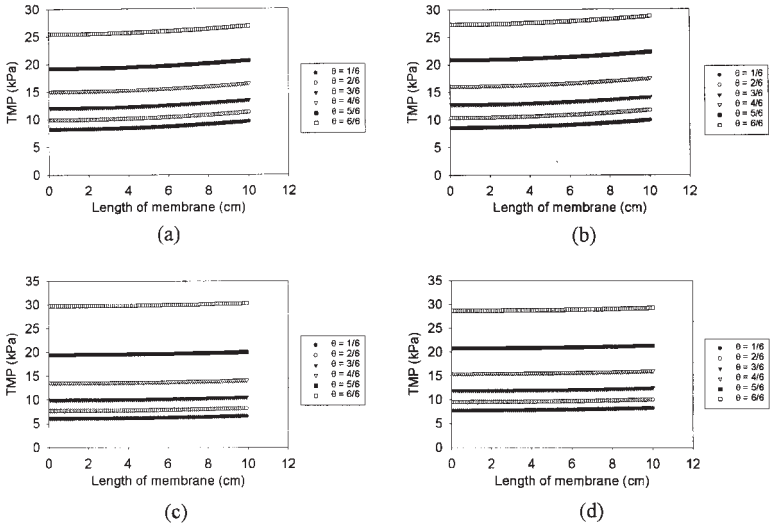

Figure 8. TMP distribution along the membrane length: (a) a 0.1-μm membrane, 1.5 g/L starch concentration; (b) a 0.1-μm membrane, 4.0 g/L starch concentration; (c) a 0.4-μm membrane, 1.5 g/L starch concentration; and (d) a 0.4-μm membrane, 4.0 g/L starch concentration.

However, the pressure differences of both sides were very similar, irrelevant to time. It is because at the pressure gradients that are needed to pull the fluid a constant flux of 100 LMH are the same at any time. Consequently, flux of the PE side was higher than the opposite side at the initial time of operation. As time passes, however, fouling of PE side became more extreme due to a higher TMP and the flux of the PE side becomes lower than that of SE side. On the other hand, the opposite SE side, where the applied pressure was relatively low, yielded lower flux at the beginning of the operation, however, the flux of SE side increased gradually to make up for the flux decline of PE side to maintain the average flux, 100 LMH (see Fig. 7). These can be explained on the whole with R_t values, which stand for the total resistances, as shown in Fig. 9. R_t of the PE side is always higher than the SE side and as time passes, the difference of filtration resistance between PE and SE sides grows bigger and mean value of R_t increases in size, the rate of R_t increment becomes faster. TMP profile resembles filtration resistance trend. Therefore, change of flux pattern would reflect TMP variation as mentioned. Mean values of R_t at each time course are shown in Fig. 10. From these computational calculation data, we can find the approximate distribution of TMP, flux, and filtration resistance along the membrane length, which cannot be measured directly by

MARCEL DEKKER, INC.
270 Madison Avenue, New York, New York 10016

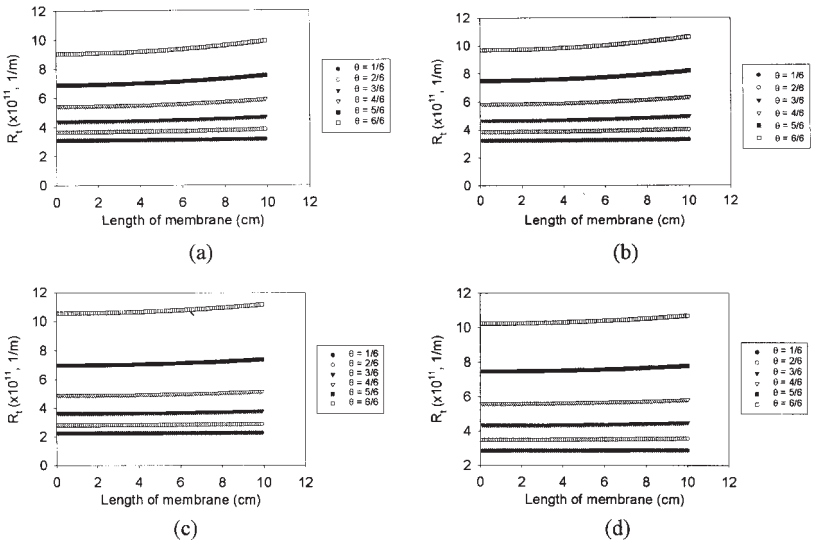

Figure 9. Total resistance distribution along the membrane length: (a) a 0.1-μm membrane, 1.5 g/L starch concentration; (b) a 0.1-μm membrane, 4.0 g/L starch concentration; (c) a 0.4-μm membrane, 1.5 g/L starch concentration; and (d) a 0.4-μm membrane, 4.0 g/L starch concentration.

experiment. Although they may not offer accurate values, these computational calculations may be used to optimize the operation conditions. It is also interesting that in flux data, all six curves cross at one point, that is, the average flux of the operation (100 LMH). In addition, that point is just the same as $x = 5.8$ cm regardless of feed concentration or membrane pore size.

Effects of Starch Concentration

To investigate the effect of starch solution concentration on the standard blocking constant, the experiments were carried out under various starch concentrations. There exists a linear relationship between K_{sb} and the concentration of feed water, as is seen in Fig. 11. However, the graph has a positive y-interception in both different pore size cases. The positive y-interception means an increase of K_{sb} compared with the case when there is no interception, i.e., membrane fouling occurs more rapidly than when we expect it according to the model equation alone. Being of y-interception reflects real errors that cannot be explained by the model alone, such as diminution of pore radius, which can make the rate of blocking pores more rapid, induced by membrane pore

Marcel Dekker, Inc.
270 Madison Avenue, New York, New York 10016

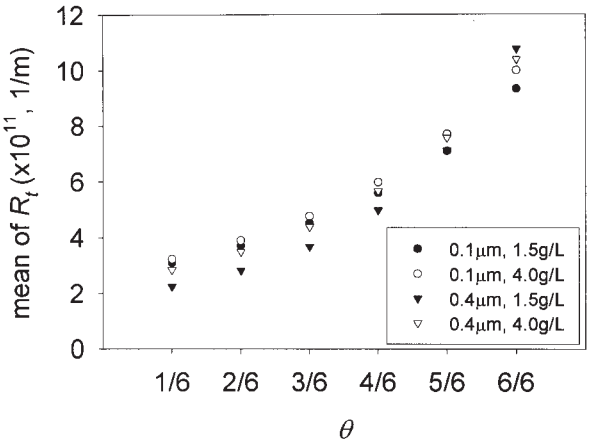

Figure 10. Mean values of R_t at each time course.

distortion resulting from TMP on pores. Faster pore blocking also can be caused by bigger foulants than normal foulants, which brings internal standard blocking. In fact, the particle size of starch solution has a distribution, a slight cake layer was found after completion of the operation. There may be another blocking mechanism, such as cake filtration and complete blocking. The membrane pores are not accurately in cylindrical form, so it is hard to say that the equation stands for a real system perfectly and indispensable errors may occur. These errors can be assembled in just one additional simple term, which takes the form of an interception of a graph.

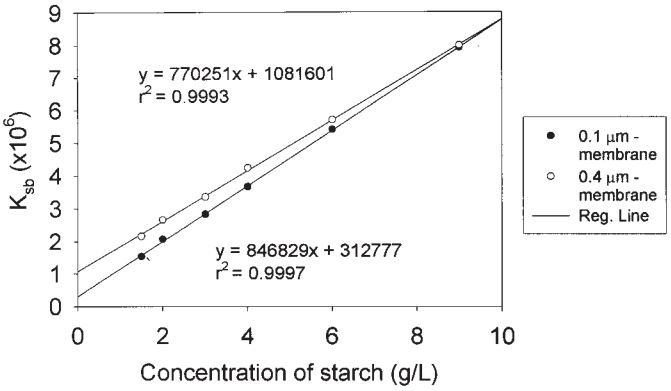

Figure 11. K_{sb} vs. concentration of the starch solution.

MARCEL DEKKER, INC.
270 Madison Avenue, New York, New York 10016

Therefore, if two K_{sbS} are given at two different concentrations, a line can be obtained, where the K_{sbS} of another concentration are accurately known without laborious experiment. K_{sb} of the target concentration can be known by just reading the graph, then, the approximate time when the operation should be terminated can be easily expected.

Effect of Pore Size

K_{sb} is inversely proportional to r_0^2, as expressed in Eq. (14). Therefore, it is easily predicted that the K_{sb} ratio has a value near $1/16$ when the initial pore radius (r_0) becomes four times larger. However, a real value of K_{sb} ratio obtained from experimental results is about 1, which is much different from our simple expectation. It is attributed to the fact that other conditions, such as number of pores (N^*) and the length of a cylindrical pore (l) of two membranes are not same, all conditions should be treated in calculation. If the model equation represents a real fouling mechanism in a good manner, the left side of Eq. (14), which is acquired by putting the K_{sb} value that is obtained by TMP curve fitting, should be identical to the right side of Eq. (14), which can be obtained by using real membrane characteristics data.

The ratio of K_{sb} slopes can be written as:

$$\frac{(\text{slope\_of\_K}_{sb})_4}{(\text{slope\_of\_K}_{sb})_1} = \frac{2C_4/\pi l_4 N_4^* r_{04}^2}{2C_1/\pi l_1 N_1^* r_{01}^2} = \frac{C_4}{C_1} \times \frac{l_1}{l_4} \times \frac{N_1^*}{N_4^*} \times \frac{r_{01}^2}{r_{04}^2}$$

$$= \frac{l_1}{l_4} \times \frac{N_1^*}{N_4^*} \times \frac{r_{01}^2}{r_{04}^2} \tag{20}$$

In Eq. (19), $C_4 = C_1$ because the comparison is performed under the same concentration of feed water.

$$\frac{l_1}{l_4} \times \frac{N_1^*}{N_4^*} \times \frac{r_{01}^2}{r_{04}^2} = R_{cal} \tag{21}$$

$$\frac{(\text{slope\_of\_K}_{sb})_4}{(\text{slope\_of\_K}_{sb})_1} = R_{fit} \tag{22}$$

where subscripts 1 and 4 stand for each pore size (1 for 0.1 μm and 4 for 0.4 μm membranes, respectively). R_{cal} and R_{fit} mean ratio of calculation values based on the experimental measurement values and ratio of values obtained by fitting, respectively.

l and r_0^2 values are given by the membrane maker (Mitsubishi Rayon). Indeed, l was measured from scanning electron microscopic (SEM) images of a cross-section of hollow fiber (Fig. 12). To get an SEM image, a clean

MARCEL DEKKER, INC.
270 Madison Avenue, New York, New York 10016

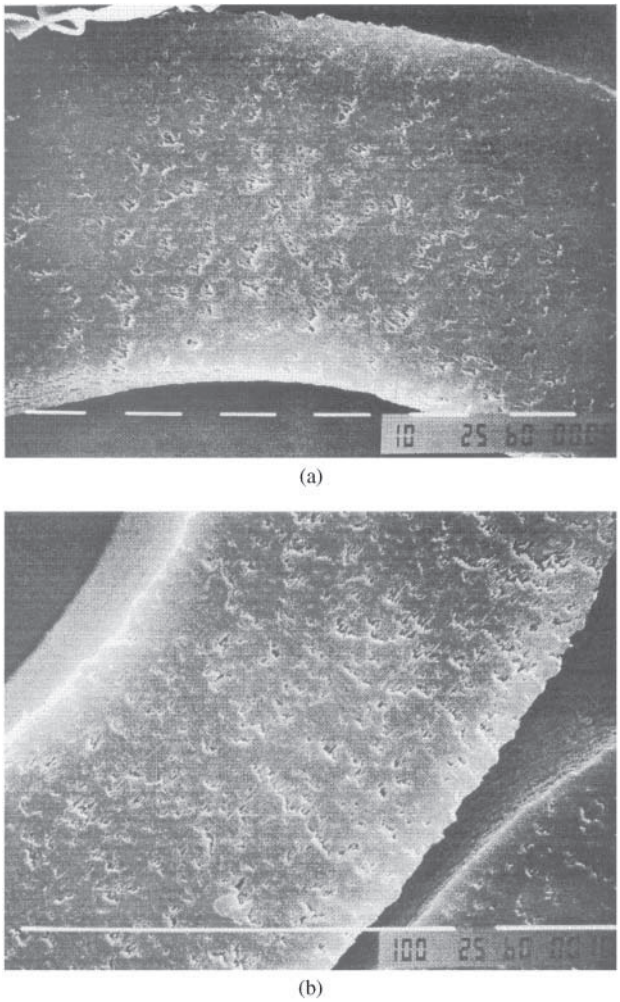

Figure 12. Scanning electron microscope of cross-sectional images of (a) a 0.1-μm hollow fiber membrane and (b) a 0.4-μm hollow fiber, membrane (outer sparse texture is a cork).

cross-section of membrane was needed. So, the hollow fibers were stitched into a cork, fixed by a fixative, such as Colloidon, then cut into slices.[12] It is clear that the hollow fiber membranes used in this experiment had no skin layer (confirmed by personal communication with Mitsubishi Rayon).[13] Therefore, the difference of the outer radius and inner radius replaces the length of skin

MARCEL DEKKER, INC.
270 Madison Avenue, New York, New York 10016

layer for calculation of l, 68.0 μm for a 0.1-μm membrane and 88.6 μm for a 0.4-μm membrane from the SEM images (see Fig. 12).

With the N^* values listed in Tables 3 and 4, and the length of pore (l), the value of R_{cal} can be calculated,

$$R_{cal} = \frac{(68.0\,\mu m)}{(88.6\,\mu m)} \times \frac{(8.095 \times 10^{15})}{(1.987 \times 10^{15})} \times \frac{(0.22\,\mu m/2)^2}{(0.41\,\mu m/2)^2} = 0.90$$

and the values of R_{fit} are shown in Fig. 13, which contains ratio data of K_{sb} of 0.4 μm to K_{sb} of 0.1 μm, calculated at each concentration of starch solution with use of the real K_{sb} values obtained by least squares fitting. It was found that R_{fit} has a range of 0.88–0.94, as shown in Fig. 13. This results from the fact that K_{sb} values are not exactly on the linear line but have little differences at each concentration. Because new membranes were used at each concentration, the characteristics of the membranes could not be exactly the same (i.e., different pore sizes, pore numbers, and pore length), which can affect K_{sb} value composition and K_{sb} itself cannot fully satisfy real TMP profile (r^2 values of linear regression are not exactly 1.). Considering these factors, it can be said that extent of errors is acceptable. Furthermore, the order of K_{sb} is so large that some extent of deviation of the K_{sb} value from the regression line hardly affects the regression line.

If all K_{sb} values fall exactly in one regression line, R_{fit} will have only one value, which is the ratio of the slopes of two cases (770251/846829 = 0.91). This value differs from R_{cal}(0.90) by only 1%. Therefore, it can be said that the K_{sb} value can be predicted with the use of R_{cal}. The approximate pattern of TMP increase can also be known easily using R_{cal} in the case when the initial pore size of membrane is different. The fact that the K_{sb} ratio is near 1 means that in case of

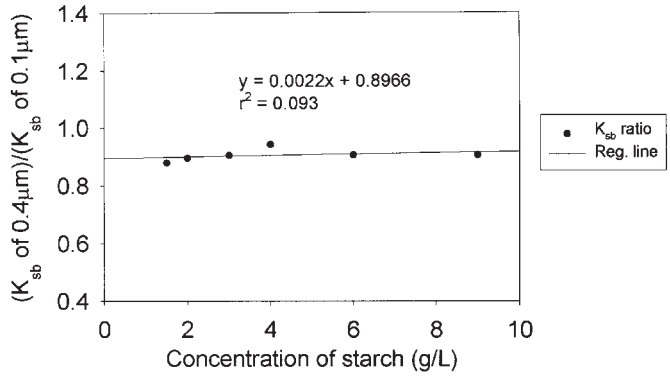

Figure 13. Ratio of K_{sb} (0.4 μm) to K_{sb} (0.1 μm) at each concentration of starch solution.

MARCEL DEKKER, INC.
270 Madison Avenue, New York, New York 10016

hollow fiber MF membranes that are on sale in markets, membranes of different pore size do not have much different filtration times at the same feed concentration.

CONCLUSION

The filtration characteristics and possibilities of TMP variation prediction in submerged microfiltration were examined in the case of different feed concentrations and different initial membrane pore sizes, both theoretically and experimentally. The following conclusions are drawn.

1. In case of submerged-type microfiltration of starch solution, with an R_f much bigger than R_c, we can conclude that there is little effect of cake filtration but the internal fouling mechanism (standard blocking) is dominant. TMP variation prediction model developed based on the standard blocking model equation was confirmed to quite accurately estimate the TMP profile of various feed concentrations and different pore sizes.
2. Distribution of TMP, flux, and total resistance along the membrane length at each time course, which can be measured hardly directly by way of experiments, were estimated and figured out respectively, from the computational calculation based on the model developed. From the figures, we could find that the flux of the potted area close to a suction pump was initially higher than the opposite side of membrane. However, total resistance of potted area was always higher than the opposite side, as time passed by, the flux of PE area became lower than the opposite side, i.e., the flux inversion phenomenon occurred, which was not expected. Also, TMP distribution along the membrane length could give us information that the potted area of membrane is more fouled and should be cleaned further than the other part. That may lead to more effective and economical operation.

NOMENCLATURE

C	Volume of particles deposited by unit volume of filtrate (—)
D	Fibre diameter (m)
d	Pore diameter (m)
g	Gravitational acceleration ($m\,sec^{-2}$)
J	Permeate flux ($m\,sec^{-1}$)
k	Hydrodynamic permeability (sec^{-1})

MARCEL DEKKER, INC.
270 Madison Avenue, New York, New York 10016

L	Fiber length (m)
l	Pore length (m)
L_p	Length of potted area (m)
L_t	Length of tubing between the end of potted area and where the pressure gauge is located (m)
n	Number of pores (—)
N^*	Total number of pores (—)
p	Pressure (Pa)
p_f	Pressure at the exit of membrane module (Pa)
p_p	Pressure at the beginning of potted area (Pa)
Q	Flow rate ($m^3\,sec^{-1}$)
r	Radius of decreased pore (m)
v	Average velocity ($m\,sec^{-1}$)
V_F	Filtrate volume (m^3)
R	Resistance (m^{-1})
R_f	Fouling resistance (m^{-1})
K_{sb}	Standard blocking model constant (m^{-3})
r^2	Coefficient of determination (—)
ρ	Density of the fluid that passes through the lumen ($kg\,m^{-3}$)
μ	Viscosity of the fluid (Pa sec)
δ	Interfacial tension ($Pa\,m^{-1}$)

Subscripts

0	Initial
avg	Average
c	Cake
i	Inner
m	Membrane
o	Outer
t	Total

ACKNOWLEDGMENTS

The authors would like to thank the Korean Ministry of Sciences and Technology for the financial support under grant M6-0203-00-0021. We also thank Sung-Hoon Yoon for assistance in helpful advice about organizing MATLAB codes. Mitsubishi Rayon Co., Japan is appreciated for providing us with membrane modules used in this work.

REFERENCES

1. National primary drinking water regulations; disinfections/disinfection by-products (proposed rule). Fed. Reg. **1994**, *59* (145), 38,668, US EPA.
2. European Membrane Society. *Membrane Processes in Water and Wastewater Treatment*; XVth Annual Summer School, Toulouse, France, July 6–10, 1998.
3. Shimizu, Y.; Uryu, K.; Okuno, Y.; Ohtubo, S.; Watanabe, A. Effect of particle size distributions of activated sludges on cross-flow microfiltration flux for submerged membranes. J. Fermen. Bioeng. **1997**, *83* (6), 583–589.
4. Chellam, S.; Jacangelo, J.G.; Banacquisti, T.P. Modeling and experimental verification of pilot-scale hollow fiber, direct flow microfiltration with periodic backwashing. Environ. Sci. Technol. **1998**, *32*, 75–81.
5. Hermia, J. Constant pressure blocking filtration laws-application to power-law non-newtonian fluids. Trans. IChemE **1982**, *60*, 183–187.
6. Fujita, H. Simulation of membrane fouling and estimation of the efficiency of operation methods in external type hollow fiber membrane. Jpn. Water Works Assoc. **1995**, *64* (3), 12–23 (in Japanese).
7. Cho, D.C.; Yoon, S.H.; Kim, H.S.; Kim, J.Y.; Kwon, S.H.; Ahn, K.H. The quantitative evaluation of the effectiveness of operation method using membrane fouling coefficient in submerged membrane filtration. J. Korean Soc. Environ. Eng. **1999**, *21* (5), 887–895 (in Korean).
8. Lee, S.H.; Kim, J.H.; Lee, C.H. Analysis of $CaSO_4$ scale formation mechanism in various nanofiltration modules. J. Membr. Sci. **1999**, *163*, 63–74.
9. Capannelli, G.; Vigo, F.; Munari, S. Ultrafiltration membranes—characterization methods. J. Membr. Sci. **1983**, *15*, 289–313.
10. Chung, K.Y.; Chang, K.M.; Seo, S.J. Determination of microfiltration fouling characteristics by liquid displacement methods. Membr. J. **1999**, *9* (4), 221–229 (in Korean).
11. Kesting, R.E. *Synthetic Polymreic Membranes*; McGraw-Hill: New York, 1971.
12. Kim, N.S.; Kim, S.R. *Clothing Arrangement*; Korea National Open University Press; 1998; 376–379.
13. Mittubishi Rayon (Naoya Tankamaru, manager, e-mail: tanakamaru_na@mrc.co.jp), personal communication.

Received June 2003

MARCEL DEKKER, INC.
270 Madison Avenue, New York, New York 10016